Hereditary hemochromatosis disrupts uric acid homeostasis and causes hyperuricemia via altered expression/activity of xanthine oxidase and ABCG2

Bojana RISTIC, Sathish SIVAPRAKASAM, Monisha NARAYANAN and Vadivel GANAPATHY

Department of Cell Biology and Biochemistry, Texas Tech University Health Sciences Center, Lubbock, TX, 79430. USA

Address correspondence to Dr. Vadivel Ganapathy at the Department Cell Biology and Biochemistry, MS 6540, 3601 4th Street, Lubbock, TX, 79430, USA. Phone: (806) 743-2518. E-mail: vadivel.ganapathy@ttuhsc.edu

Abstract

Hereditary hemochromatosis (HH) is mostly caused by mutations in the iron-regulatory gene *HFE*. The disease is associated with iron overload, resulting in liver cirrhosis/cancer, cardiomegaly, kidney dysfunction, diabetes, and arthritis. Fe^{2+}-induced oxidative damage is suspected in the etiology of these symptoms. Here we examined, using *Hfe*$^{-/-}$ mice, whether disruption of uric acid (UA) homeostasis plays any role in HH-associated arthritis. We detected elevated levels of UA in serum and intestine in *Hfe*$^{-/-}$ mice compared to controls. Though the expression of xanthine oxidase, which generates UA, was not different in liver and intestine between wild type and *Hfe*$^{-/-}$ mice, the enzymatic activity was higher in *Hfe*$^{-/-}$ mice. We then examined various transporters involved in UA absorption/excretion. Glut9 expression did not change; however, there was an increase in Mrp4 and a decrease in Abcg2 in *Hfe*$^{-/-}$ mice. As ABCG2 mediates intestinal excretion of UA and mutations in ABCG2 cause hyperuricemia, we examined the potential connection between iron and ABCG2. We found p53-responsive elements in h*ABCG2* promoter and confirmed with chromatin immunoprecipitation that p53 binds to this promoter. p53 protein was reduced in *Hfe*$^{-/-}$ mouse intestine. p53 is a heme-binding protein and p53-heme complex is subjected to proteasomal degradation. We conclude that iron/heme overload in HH increases xanthine oxidase activity and also promotes p53 degradation resulting in decreased ABCG2 expression. As a result, systemic UA production is increased and intestinal excretion of UA via ABCG2 is decreased, causing serum and tissue accumulation of UA, a potential factor in the etiology of HH-associated arthritis.

Key Words: Hemochromatosis, *Hfe*-null mouse, iron/heme overload, tumor suppressor p53, ABCG2, hyperuricemia

Short title: Hyperuricemia in hemochromatosis via iron/heme-p53-ABCG2 axis

Summary Statement

Deletion of the iron-regulatory gene *Hfe* leads to hyperuricemia via heme-induced degradation of p53 and consequent silencing of *ABCG2* expression; these findings have relevance to the etiology of arthropathy, a common symptom in patients with the iron-overload disease hemochromatosis.

Introduction

Uric acid (UA), the ubiquitous end-product of purine catabolism, is an intriguing molecule whose biochemical and pathological effects are dictated by its concentration and the surrounding microenvironment. UA is one of the major endogenous antioxidants whose action is directed towards prevention of lipid peroxidation and inactivation of nitric oxide synthase [1]. In addition, UA is a potent iron chelator; it minimizes iron-mediated redox reactions and generation of reactive oxygen species (ROS) [2]. However, this is true only when UA is present in physiologic concentrations, which is 3.5 – 7.2 mg/dL in adult males and postmenopausal females and 2.6 – 6.0 mg/dL in premenopausal women [3]. However, the antioxidant capacity of UA is overshadowed by detrimental effects when its concentration exceeds its maximal solubility (6-7 mg/dL) [4]. In this scenario, UA precipitates and crystalizes as monosodium urate (MSU), which gets deposited in joints, leading to inflammation and gouty arthritis [5]. Since there is an overlap in UA concentrations that define hyperuricemia and that dictate MSU crystal formation, and both have pathological implications, recent discussions continue to emphasize the need for reduction of this "healthy" UA range [3].

Origin of inflammation caused by MSU crystals is multifactorial. MSU crystals in synovium are engulfed by neutrophils/monocytes where they initiate ROS production and cell death [5]. In addition, they communicate with resident macrophages; upon encounter, MSU crystals trigger the assembly of NLRP3-inflammasome in macrophages and stimulate production and secretion of the proinflammatory cytokine interleukin-1β [5]. Ultimately, the proinflammatory cytokine storm, accumulation of ROS, and acute (later chronic) flares and excruciating joint pain constitute the pathophysiology of gout [4]. The levels of UA in circulation are dictated by the balance between the rate of its production and the rate of its excretion, and genetics is an important determinant in this phenomenon. Recently we reviewed the genetic defects in various transporters that play a critical role in UA homeostasis, consequently leading to either hypouricemia or hyperuricemia [6].

An additional risk factor for arthritis is iron [7] because free iron participates in redox reactions by acting as an electron donor and receptor, ultimately leading to production of hydroxyl radicals and oxidative damage [8]. If that occurs in synovium, arthritis-like symptoms appear [9]. Hereditary hemochromatosis (HH) is considered to be the most prevalent disease associated with iron overload; it affects 1 in 250 individuals in certain populations [11]. It is usually referred to as a "silent disease" because iron loading and iron-elicited damages occur gradually, and detrimental symptoms appear only at 50-60 years of age [12]. In about 80% of cases, HH is caused by autosomal recessive mutations in *HFE* gene, with C282Y being the most prevalent mutation [13]. HFE, a major histocompatibility class-I-like plasma membrane protein [14], is a critical component of iron-sensing and iron homeostasis-regulatory complex. Its action is mediated by promotion of the synthesis of hepcidin, a hepatic hormone that regulates the amount of iron that enters circulation from diet and tissue-resident macrophages [15]. Missense mutations in *HFE* disrupt the iron-sensing complex and leads to ablation of hepcidin production [16]; this causes systemic iron overload and iron deposition in multiple organs [17]. As a result of iron deposition and iron-induced oxidative damage, the disease manifests with dysfunction of multiple organs, causing liver cirrhosis and liver cancer, nephropathy, cardiomegaly, diabetes, and pituitary insufficiency.

Arthropathy is commonly seen in patients with HH [18-23]. Iron accumulation and consequent oxidative damage are believed to be the principal cause of joint damage in HH. Calcium pyrophosphate dihydrate crystals are found in affected joints, imitating pseudogout [24] and free iron reduces the clearance of these deposits from joints [25]. There are no published reports linking HH to dysregulation of UA homeostasis; this is intriguing given the well-established role of excess UA in arthritis. This critical knowledge gap renders our current understanding of arthropathy in HH incomplete. Therefore, we examined UA status in HH using a mouse model of HH, namely *Hfe*$^{-/-}$ mouse. These studies demonstrate that *Hfe*$^{-/-}$ mice have hyperuricemia and that decreased excretion of UA in the intestine via down-regulation of the UA exporter ABCG2 is likely to be the principal contributor to this phenomenon.

Materials and Methods

Animals

Hfe$^{-/-}$ mice on C57BL/6 background were purchased from Jackson Laboratory (Bar Harbor, ME, USA) and C57BL/6 *Abcg2*$^{-/-}$ mice were purchased from University of California Davis Knockout Mouse Project (KOMP) Repository (Davis, CA, USA). The mice were maintained at the animal facility of Texas Tech University Health Sciences Center (TTUHSC) in a temperature- and light-controlled environment, with water and laboratory rodent diet provided ad-libitum. Male and female mice older than 7 months were used in this study. The control mice matched the background strain, age and gender of the experimental groups. All experimental procedures were approved by the TTUHSC Institutional Animal Care and Use Committee (IACUC – protocol number 18005) and the Institutional Review Board (IRB). For tissue collection, mice were killed by cervical dislocation under CO_2 anesthesia in accordance with the guidelines from the American Veterinary Medical Association.

Cell Culture

Normal human colonic epithelial cell line, CCD841, was purchased from American Type Culture Collection (ATCC, Manassas, VA, USA). The cell line was cultured in RPMI 1640 (Corning, Corning, NY, USA) supplemented with 10% FBS (Fisher Scientific, Pittsburgh, PA, USA) and 1% penicillin/streptomycin (Corning, Corning, NY, USA). Viral packaging cell line, HEK293FT, was purchased from ATTC (Manassas, VA, USA) and maintained in DMEM 4.5 g/L glucose, L-glutamine, sodium pyruvate (Corning, Corning, NY, USA) supplemented with 10% FBS and 1% penicillin/streptomycin. HEK293FT cells were used for transient transfection experiments where they were cultured for three passages in the presence and absence of excess iron in the form of ferric ammonium citrate (FAC) (Sigma, St. Louis, MO, USA) [26] and then used for ectopic expression of p53.

Antibodies

Anti-ABCG2 (D5V2K XP®, #42078) and anti-p53 (1C12, #2524) monoclonal antibodies were purchased from Cell Signaling Technology (Danvers, MA, USA). Anti-β-actin (C4, sc-47778) and anti-β-tubulin (D-10, sc-5274) monoclonal antibodies were purchased from Santa Cruz Biotechnology (Dallas, TX, USA). Anti-xanthine oxidase monoclonal antibody (EPR4605, ab109235) was purchased from Abcam (Cambridge, MA, USA) and anti-GLUT9 polyclonal

antibody (PA5-22966) was purchased from Thermo Fisher Scientific (Waltham, MA, USA). Horseradish peroxidase-conjugated goat anti-rabbit (#1706515) and goat anti-mouse (#1706516) were purchased from Bio-Rad Laboratories (Hercules, CA, USA).

Measurement of UA

The UA content of the intestinal tissue and serum was measured by the fluorimetry-based Uric Acid Assay Kit (Abcam, Cambridge, MA, USA), as described by the manufacturer. The UA concentration of the tissue was recorded as nmol of UA per milligram of protein, while the serum concentration was recorded as nmol of UA per ml of serum.

Measurement of serum creatinine

Creatinine concentration in serum was measured by the fluorimetry-based Creatinine Assay Kit (Biovision, Milpitas, CA, USA) as per manufacturer's protocol. The creatinine concentration was recorded as mg/dl of serum.

Measurement of uricase activity

Uricase activity in liver and colon was measured by the fluorimetry-based Amplex® Red Uric Acid/Uricase Assay Kit (Thermo Fisher Scientific, Waltham, MA, USA) as per manufacturer's protocol. Uricase activity was recorded as mU/mg protein. One unit is defined as the amount of enzyme that will convert 1 μmole of uric acid to allantoin per min at pH 8.5 and 25 ℃.

Measurement of XO activity

XO activity in liver and jejunum was measured by fluorimetry-based XO Activity Assay Kit (Sigma, St. Louis, MO, USA) as per manufacturer's protocol. XO activity was recorded as nmol of H_2O_2 generated per minute per milligram of protein.

RNA isolation and quantitative PCR

Total RNA from animal tissues and cultured cells was extracted using TRIzol reagent (Thermo Fisher Scientific, Waltham, MA, USA). RNA purity and concentration were quantified using NanoDrop Spectrophotometer 2000 (Thermo Fisher Scientific, Waltham, MA, USA). 2 μg of RNA was reverse transcribed into cDNA using the SuperScript III First-Strand cDNA synthesis kit (Thermo Fisher Scientific, Waltham, MA, USA). Relative mRNA levels were measured with StepOne Plus real-time PCR system (Applied Biosystems, Foster City, CA, USA) using the SYBR® Green supermix (Bio-Rad Laboratories, Hercules, CA, USA), and were normalized to the housekeeping gene HGPRT (hypoxanthine/guanine phosphoribosyl transferase). The PCR primer sequences are given in Supplementary Table S1.

Protein isolation and western blot

For whole tissue/cell extract preparation, tissues and cells were lysed in Pierce™ RIPA buffer (Thermo Fisher Scientific, Waltham, MA, USA) supplemented with Halt™ Protease and Phosphatase Inhibitor Cocktail (Thermo Fisher Scientific, Waltham, MA, USA). Homogenates were centrifuged, and supernatants were used for protein measurement via Pierce™ BCA Protein

Assay Kit (Thermo Fisher Scientific, Waltham, MA, USA). Western blot samples were prepared in Laemmli Sample Buffer (Bio-Rad Laboratories, Hercules, CA, USA). They were loaded onto a 10% SDS-polyacrylamide gel electrophoresis (SDS-PAGE) gel and transferred onto a PVDF membrane (Bio-Rad Laboratories, Hercules, CA, USA). The membrane was blocked, and antibodies diluted in 5% nonfat dry milk (Bio-Rad Laboratories, Hercules, CA, USA) or in 5% bovine serum albumin (Irvine Scientific, Santa Ana, CA, USA) were used. Protein bands were visualized using Pierce™ ECL Western Blotting Substrate (Thermo Fisher Scientific, Waltham, MA, USA) and developed on the autoradiography film (Santa Cruz, Dallas, TX, USA).

Isolation of ileal and colonic mucosal epithelial cells

Ileum and colon were cut open longitudinally, washed with ice-cold phosphate-buffered saline and placed on an ice-cold glass surface with the lumen side facing up. The epithelium was mechanically detached and collected by scraping with the glass slide. Samples were centrifuged and the pellet was used for further analysis.

Lentiviral transfection

Construct for shRNA to degrade p53 mRNA (pLKO-p53-shRNA-427; Addgene plasmid # 25636) was created by Todd Waldman laboratory and purchased from Addgene plasmid repository (Watertown, MA, USA) [27]. pLKO.1 empty vector was used as a control. To generate transient virus stock, HEK293FT cells were plated in 10-cm dish and allowed to reach 100% confluency. 7.5 µg of control, shRNA vector, and packaging plasmids (PLP1, PLP2, and VSVG) were delivered to the cells using Lipofectamine-2000 reagent (Thermo Fisher Scientific, Waltham, MA, USA). 48 h after transient transfection, the virus-containing medium was harvested, centrifuged and filtered to generate virus stock. CCD841 cells were seeded in 6-well plates; they were at 50% confluency on the day of the infection. Virus stock contained 8 µg/ml of polybrene to increase the transduction efficacy. 48 h after infection, desired clones were selected by administration of puromycin (1 µg/ml).

Chromatin immunoprecipitation assay

ChIP assays were performed using EZ-Magna ChIP A/G kit (Millipore, Burlington, MA, USA) according to the manufacturer's instructions. Briefly, cells were cross-linked with 1% formaldehyde, collected in phosphate-buffered saline supplemented with Halt™ Protease and Phosphatase Inhibitor Cocktail (Thermo Fisher Scientific, Waltham, MA, USA) and lysed in nuclear lysis buffer. The lysate was then sonicated using BioRuptor Plus (Diagenode, Denville, NJ, USA) to shear DNA into fragments of approximately 200-1,000 base pairs. DNA concentration was measured using NanoDrop Spectrophotometer 2000 (Thermo Fisher Scientific, Waltham, MA) and 25 µg of DNA was used for immunoprecipitation with anti-p53 antibody or normal mouse IgG. Before immunoprecipitation, 1% of the supernatant was removed as an input. DNA was isolated on the column and relative enrichment of p53 on h*ABCG2* gene promoter was assessed via real-time quantitative PCR. The PCR primer sequences are provided in Supplementary Table S1.

Transient transfection

Construct for wild type p53 (pcDNA3 p53 WT; Addgene plasmid # 69003) was purchased from Addgene plasmid repository (Watertown, MA, USA) [28]. pcDNA3 empty vector was used as a control. HEK293FT cells were cultured first for three passages in the absence or presence of FAC (250 μg/ml) and then used for transient ectopic expression of p53. Control and iron-overloaded cells were plated in 6-well plates and allowed to reach 80-90% confluency. 2.5 μg of control and p53 WT plasmids were delivered to the cells using Lipofectamine-3000 reagent (Thermo Fisher Scientific, Waltham, MA, USA). Ferric ammonium citrate was absent during the transfection step, but was added to the culture medium after that step. 48 h later, RNA and protein lysates were prepared.

Statistical analysis

Experiments were repeated at least three times. The data shown are representative results of the means ± SEM. Statistical analyses and graphing were performed using GraphPad Prism 7.01 software. Statistical differences between control and experimental groups were analyzed by a two-tailed, unpaired Student's t-test for single comparison. Differences were judged statistically significant when the p value < 0.05.

Results

Hfe$^{-/-}$ mouse exhibits hyperuricemia

To assess if HH leads to the development of hyperuricemia, we measured systemic and organ-specific UA concentration in *Hfe*$^{-/-}$ mice. We found that, when compared to the wild type, *Hfe*$^{-/-}$ mice had elevated UA in the circulation (Figure 1A). As the large intestine and mid-to-distal parts of the small intestine are involved in UA homeostasis, contributing to at least 40% to total UA excretion, we monitored UA levels in *Hfe*$^{-/-}$ intestine. Compared to the control, *Hfe*$^{-/-}$ ileum (Figure 1B) and colon (Figure 1C) had a significantly higher accumulation of UA.

Besides the intestinal tract, UA is excreted by the kidneys [29]; as such, renal dysfunction is also a significant determinant of circulating levels of UA. Therefore, we investigated if the observed UA accumulation in serum was due to the impaired glomerular filtration in HH. We estimated the glomerular filtration rate in wild type mice and *Hfe*$^{-/-}$ mice in an indirect manner by measuring the concentration of creatinine in circulation. If the body weight is comparable between the two groups, creatinine levels in blood serve as a surrogate for glomerular filtration rate. For this, we used only male mice; mice in both genotype groups had comparable body weight (Supplementary Figure S1A). We found that the serum creatinine levels did not differ between the two groups (Supplementary Figure S1B), suggesting that there is no difference in glomerular filtration rate between wild type and *Hfe*$^{-/-}$ mice (males, 7-month-old).

Uricase expression and activity in wild type and *Hfe*$^{-/-}$ mice

The hyperuricemia in *Hfe*$^{-/-}$ mice can be due to overproduction, degradation, or underexcretion of UA, or a combination of some or all. To discern the underlying mechanism of UA elevation, we first investigated the expression and activity of uricase (also called urate oxidase), an enzyme that oxidizes UA into allantoin in rodents, but is absent in humans and other higher primates due to the

non-functional pseudogene [30]. Quantitative PCR analyses showed no significant difference in the mRNA expression of uricase between two genotypes (Supplementary Figure S2A). In addition, deletion of *Hfe* gene did not alter uricase activity (Supplementary Figure S2B).

Increased enzymatic activity of xanthine oxidase in *Hfe*$^{-/-}$ mouse

Next, we investigated the expression levels and the activity of xanthine oxidase (XO), the enzyme that catalyzes the terminal reaction in UA synthesis [31]. XO is expressed in mouse liver and small intestine, with the highest levels present in jejunum (Figure 2A). On the protein level, however, XO was most abundant in liver; its levels were much less in the intestinal tract and it decreased aborally (Figure 2B). This expression pattern did not differ between wild type and *Hfe*$^{-/-}$ mice, except for liver, where XO mRNA decreased in *Hfe*$^{-/-}$ mice (Figure 2C, D). Since XO active site contains molybdenum and iron as cofactors [32], we pondered whether excess iron alters XO enzyme activity. We measured XO enzymatic activity in liver and jejunum of wild type and *Hfe*$^{-/-}$ mice. We found a significant increase in XO activity in *Hfe*$^{-/-}$ liver and jejunum (Figure 2E).

Glut9 and Mrp4 expression in *Hfe*$^{-/-}$ mouse

We then monitored the expression levels of the transporters that are involved in absorption and excretion of UA in liver and intestine in wild type and *Hfe*$^{-/-}$ mice. We first focused on two transporters: a passive, bidirectional UA carrier GLUT9 (also known as SLC2A9) and an ATP-dependent unidirectional UA exporter MRP4 (ABCC4). These transporters are expressed on apical and basolateral membranes in hepatocytes and enterocytes [33]. Glut9 mRNA expression was comparable between liver and jejunum of the wild type mice, but it was significantly lower in ileum and colon (Figure 3A). On the contrary, protein levels differed significantly, with Glut9 primarily detectable in the intestinal tract (Figure 3B). More relevant to the current study is the finding that deletion of *Hfe* did not influence the levels of Glut9 mRNA or protein (Figure 3C, D). Mrp4 was expressed highly in liver and colon; its expression increased aborally in the intestinal tract (Figure 3E). When compared to wild type mice, Mrp4 mRNA levels were lower in the liver, but significantly higher in the jejunum and colon of *Hfe*$^{-/-}$ mice (Figure 3F).

Abcg2 expression in wild type mouse and impact of *Abcg2* deletion on UA in circulation

UA is a substrate for the ATP-dependent export pump ABCG2 [34]; the transporter is responsible for most of intestinal excretion of UA. Abcg2 mRNA was found in kidney, liver and intestinal tract, highest level of expression noted in jejunum and ileum (Figure 4A). Abcg2 protein was highest in jejunum, and it decreased in the intestinal tract aborally (Figure 4B). In a genome-wide association study, Woodward et al. [35] identified multiple SNPs in *ABCG2* to be associated with hyperuricemia and gout. The Q141K mutation decreases the transport function of ABCG2 by ~50% [35]. This phenomenon is phenocopied in *Abcg2*$^{-/-}$ mice, where complete deletion of *Abcg2* gene resulted in elevated UA levels in circulation (Figure 4C).

Downregulation of Abcg2 in the intestinal tract of *Hfe*$^{-/-}$ mice

As hyperuricemia was found in *Hfe*$^{-/-}$ mice as well as in *Abcg2*$^{-/-}$ mice, we became curious about a possible connection between HFE and ABCG2. We hypothesized that Abcg2 expression is decreased in HH, thus providing a molecular basis of hyperuricemia in *Hfe*$^{-/-}$ mice. To test this hypothesis, we monitored the expression levels of Abcg2 mRNA and protein in ileum and colon

between wild type and *Hfe*$^{-/-}$ mice, specifically in the mucosal epithelium. Abcg2 mRNA was significantly lower in *Hfe*$^{-/-}$ colon (Figure 5A). The Abcg2 protein levels were also lower in ileum and colon in *Hfe*$^{-/-}$ mice (Figure 5B-D). The decrease was ~5-fold in ileum and ~3-fold in colon.

p53-mediated transcriptional regulation of ABCG2

The follow-up question that needed to be answered was: what is the mechanism underlying the Abcg2 downregulation in HH mouse? 5'-UTR of h*ABCG2* and m*Abcg2* is located in exon1 and is alternatively spliced to translation start site in exon 2. There are at least 3 splice variants found in both species, which results from alternative promoter usage [36]. Colon h*ABCG2* expresses all three isoforms [37], while m*Abcg2* variants are primarily investigated in hematopoietic stem cells [38]. Analysis of the 5'-UTRs of human *ABCG2* and mouse *Abcg2* 5' revealed binding sites for p53 (Figure 6A). To test if the interaction between *ABCG2* promoter and p53 occurs in cells, we performed ChIP assay. Experiment was conducted in the normal human colonic epithelial cell line, CCD841. We generated lentiviral transfectants to silence p53 via shRNA, while empty vector was used as a control; we noted a marked decrease in ABCG2 protein levels when p53 was silenced (Figure 6B). If p53 binds to *ABCG2* promoter, the contact between the protein and the promoter would be lower in the shRNA-silenced cell line. We used a specific antibody to pull down p53, and performed quantitative PCR using primers specific for the h*ABCG2* promoter with p53 pulldown. This analysis revealed significant enrichment of *ABCG2* promoter in the p53 pulldown. The opposite trend was observed in the shRNA-silenced cell line. When p53 protein levels were lowered, the enrichment was significantly reduced (Figure 6B). The validity and dependability of the method were supported by observations that the pulldown of the p21 and GADD45A, the prototypical targets for p53, was also decreased in cells where p53 was silenced (Figure 6B).

Recent studies have shown that p53 is a heme-binding protein and that p53-heme complex is exported out of nucleus for subsequent proteasomal degradation [39]. This suggested that heme accumulation as occurs in HH might lead to downregulation of p53 in *Hfe*$^{-/-}$ mice. Therefore, we hypothesized that decreased expression of p53 is responsible for decreased expression of Abcg2 in *Hfe*$^{-/-}$ mice. We collected ileal and colonic mucosa of wild type and *Hfe*$^{-/-}$ mice and performed western blot to compare p53 protein levels between two genotypes. We found that p53 protein was significantly lower in *Hfe*$^{-/-}$ ileum than in wild type controls (Figure 7A); the reduction was ~4-fold compared to the control (Figure 7B). The same was true in *Hfe*$^{-/-}$ colon (Figure 7C, D).

Effect of p53 reconstitution on FAC-induced decrease in ABCG2 expression

Our studies show that chronic exposure to iron in colonic epithelial cells decreases p53 protein with subsequent decrease in ABCG2 mRNA. To confirm these findings further, we reconstituted p53 in FAC-exposed cells via ectopic expression to see if it would restore ABCG2 mRNA levels. Initial experiments with FAC-exposed CCD841 cells for ectopic expression of p53 failed due to low transfection efficiency. Therefore, we used HEK293FT cells, which exhibit robust transfection efficiency. We first exposed these cells to FAC (250 μg/ml) for three passages. Control and FAC-exposed cells were then used for transient ectopic expression of p53. FAC was omitted during transfection. We then monitored p53 protein levels (Western blot) and ABCG2 mRNA levels (qRT-PCR) in control and FAC-exposed cells with and without ectopic expression of p53. We observed decreased p53 protein in FAC-exposed cells compared to control cells (Supplementary Figure S3A). Under these conditions, we also observed the downregulation of ABCG2 mRNA

(Supplementary Figure S3B). Ectopic expression of p53 reconstituted this protein, both in control and FAC-exposed cells (Supplementary Figure S3A), which led to a significant recovery of ABCG2 mRNA in FAC-exposed cells (Supplementary Figure S3B). These data confirm that the decrease in ABCG2 mRNA in FAC-exposed cells is indeed due to decreased levels of p53 protein.

Discussion

In the present study, we focused on the relationship between hereditary hemochromatosis (HH) and uric acid (UA) homeostasis. The findings and implications of the present study can be summarized as follows (Figure 8). Deletion of the iron-regulatory protein Hfe causes hyperuricemia, and its origin is multifactorial. Under conditions of iron overload as occurs in HH, xanthine oxidase, which generates UA as the final step in the catabolism of purine bases, becomes more active, possibly leading to increased production of UA. In addition, the expression of the UA transporter repertoire changes significantly in the liver and intestinal tract, likely altering transmembrane transport of UA involved in removal of UA from the cells and excretion of UA into intestinal lumen. In our opinion, the most significant finding of the present study is the marked decrease in the expression of the UA exporter Abcg2 in the intestinal tract in HH. This transporter is known to be responsible for ~40% excretion of UA from the body; as such, the decreased expression of this transporter in HH is probably the major contributor to HH-associated hyperuricemia. Based on this conclusion, we investigated the molecular events underlying the downregulation of ABCG2 in HH. We showed that ABCG2 is a direct target for the tumor suppressor p53 and that the protein levels of p53 are profoundly decreased in HH. We have established the regulation of ABCG2 expression by p53 via ChIP that showed binding of p53 to h*ABCG2* gene promoter. We also showed that HH is associated with increased accumulation of heme in epithelial cells lining the ileum and colon; this is relevant to the decrease in p53 protein levels in HH. Studies by others have shown that p53 is a heme-binding protein and that p53-heme complex is a substrate for proteasomal degradation [39]. There is however some discordance between Abcg2 mRNA levels and Abcg2 protein levels in the *Hfe*$^{-/-}$ intestine; the decrease in mRNA is much less pronounced than the decrease in protein. Even though this could be explained by the often observed finding that mRNA levels do not always correspond to protein levels, the possibility of additional transcriptional control of *Abcg2* in HH by factors other than p53 cannot be excluded. The transcription factor Nrf2 is a likely candidate; Nrf2 is known to induce h*ABCG2* transcription [6], and the activity of this transcription factor is increased by oxidative stress as occurs under iron-overload conditions such as HH. Taken collectively, the results of the present study show that hemochromatosis is associated with elevated levels of UA and the iron/heme-p53-ABCG2 axis plays a critical role in this phenomenon. As arthritis is a common pathological symptom in patients with HH, the findings of the current study have profound clinical implications because they underscore the potential involvement of hyperuricemia in the pathogenesis of HH-associated arthropathy.

In contrast to the findings in our study which showed p53 as an inducer of ABCG2 expression, Wang *et al.* [40] have reported that p53 is a suppressor of ABCG2 expression, not directly but indirectly by decreasing the levels of NFκB. Our studies have shown a direct effect of p53 on ABCG2 expression as documented by the binding of p53 on h*ABCG2* gene promoter. The discrepancy between the two studies is most likely related to potential differences in the expression levels and activity status of NFκB in tissues and cell lines employed.

MRP4 has been shown to be an ATP-dependent urate exporter in a heterologous expression system using HEK293 cells [41]; however, the extent of its involvement in the maintenance of UA homeostasis in vivo in humans is not known. Although in experimental animals, knockdown of Mrp4 in kidneys cause reduction in urate export [42], there is no significant association between the *MRP4* gene polymorphism and hyperuricemia and gout occurrence in humans [43]. The only study reported in the literature on any potential association between MRP4 and UA homeostasis is that by Tanner *et al.* [44]. This study analyzed *MRP4* gene polymorphism in the settings of hyperuricemia and gout. It was found that amongst the 39 *MRP4* SNPs, only rs4148500 correlated with the hyperuricemia and gout; however, the molecular mechanism for the correlation was not explored. In the present study, we found a dramatic increase of Mrp4 mRNA levels in *Hfe*$^{-/-}$ mouse intestine, but the significance of this finding remains to be investigated. It is possible that the increase in the expression of MRP4 represents an attempt to maintain UA homeostasis as a feedback response to the downregulation of ABCG2 and the resultant increase UA levels.

To the best of our knowledge, studies by Flais *et al.* [45] is the only report in published literature that addressed hyperuricemia in HH. These investigators found that in a large cohort of patients who harbored C282Y mutation in HFE, hyperferritinemia (an evidence for iron overload) was associated with hyperuricemia occurrence. Our results are also consistent with the cross-sectional studies conducted in patients with excessive iron accumulation and hyperferritinemia where iron overload was not of a genetic origin as in HH. In these studies, increase in serum ferritin concentrations correlated positively with the increase in UA levels, and the association was independent of gender, race, age, body mass index, and alcohol consumption [46]. The same trend was seen amongst obese adolescents, irrespective of their body mass index [47]. However, these reports did not focus on the causal relationship between iron overload and hyperuricemia. In this regard, the present study is novel, because besides directly demonstrating elevated UA levels in the *Hfe*$^{-/-}$ mouse model of HH, it provides a molecular mechanism for hyperuricemia in HH.

Does the elevation in UA in HH have a beneficial effect or pathological effect? This question arises because of the dual role of UA, functioning both as an antioxidant and a pro-inflammatory agent. We opine that hyperuricemia in HH is detrimental because of the co-occurrence of free iron. UA is a chelator of iron, and free iron facilitates crystallization of monosodium urate (MSU) [48]. Besides its deposition in joints, triggering excruciating acute and chronic flares characterized in gout, MSU crystallization is associated with the development of metabolic syndrome [49], cardiovascular diseases [50], liver failure [51], and kidney failure [52]. Occurrence of these maladies is common in HH patients; therefore, our study suggests a plausible connection between hyperuricemia and the afore-mentioned broad-spectrum of organ dysfunction in HH.

In conclusion, circulating levels of UA are increased significantly in HH, potentially contributing to the known increased incidence of arthritis in this genetic disorder. Our studies uncover at least two molecular mechanisms for this HH-associated hyperuricemia, namely increased generation of UA due to increased enzymatic activity of xanthine oxidase in the liver and intestine, and decreased intestinal excretion of UA due to decreased expression of the UA exporter Abcg2 in the intestinal tract.

Abbreviations

ChIP, chromatin immunoprecipitation; FAC, ferric ammonium citrate; FBS, fetal bovine serum; HH, hereditary hemochromatosis; MSU, monosodium urate; ROS, reactive oxygen species; UA, uric acid; XO, xanthine oxidase

Author Contribution

B.R. performed most of the experiments; S.S. and M.N. made significant contribution in some experiments; V.G. designed the study and interpreted the data; V.G. and B.R. wrote the manuscript.

Funding

This work was supported by the National Institutes of Health grant R41 AR074854 and the Welch Endowed Chair in Biochemistry, Grant No. BI-0028, at Texas Tech University Health Sciences Center.

Competing Interests

The Authors declare that there is no conflict of interests associated with the manuscript.

References

1. So, A., Thorens, B. (2010) Uric acid transport and disease. *J. Clin. Invest*. **120**, 1791-1799 doi: 10.1172/JCI42344

2. Fatima, T., McKinney, C., Major, T.J., Stamp, L.K., Dalbeth, N., Iverson, C. et al. (2018) The relationship between ferritin and urate levels and risk of gout. *Arthritis Res. Ther.* **20,** 179 doi: 10.1186/s13075-018-1668-y

3. Desideri, G., Castaldo, G., Lombardi, A., Mussap, M., Testa, A., Pontremoli, R. et al. (2014) Is it time to revise the normal range of serum uric acid levels? *Eur. Rev. Med. Pharmacol. Sci*. **18,** 1295-306.

4. So, A.K., Martinon, F. (2017) Inflammation in gout: mechanisms and therapeutic targets. *Nat. Rev. Rheumatol*. **13**, 639-647 doi: 10.1038/nrrheum.2017.155

5. Desai, J., Steiger, S., Anders, H.J. (2017) Molecular pathophysiology of gout. *Trends Mol. Med.* **23,** 756-768 doi: 10.1016/j.molmed.2017.06.005

6. Ristic, B., Sikder, O.M.F., Bhutia, Y.D., and Ganapathy, V. (2020) Pharmacologic inducers of the uric acid exporter ABCG2 as potential drugs for treatment of gouty arthritis. *Asian J. Pharm. Sci*. (in press).

7. Dabbagh, A.J., Trenam, C.W., Morris, C.J., Blake, D.R. (1993) Iron in joint inflammation. *Ann. Rheum. Dis.* **52,** 67–73 doi: 10.1136/ard.52.1.67

8. Winterbournn C.C. (1995) Toxicity of iron and hydrogen peroxide: the Fenton reaction. *Toxicol. Lett.* **82/83**: 969-974.

9. Morris, C.J., Earl, J.R., Trenam, C.W., Blake, D.R. (1995) Reactive oxygen species and iron - a dangerous partnership in inflammation. *Int. J. Biochem. Cell Biol*. **27**, 109-122 doi: 10.1016/1357-2725(94)00084-O

10. Kra, S.J., Hollingsworth, J.W., Finch, S.C. (1965) Arthritis with Synovial Iron Deposition in a Patient with Hemochromatosis. *N. Engl. J. Med.* **272**, 1268-1271 doi: 10.1056/NEJM196506172722404

11. Merryweather-Clarke, A.T., Pointon, J.J., Shearman, J.D., Robson, K.J.H. (1997) Global prevalence of putative haemochromatosis mutations. *J. Med. Genet.* **34,** 275-278 doi: 10.1136/jmg.34.4.275

12. Adams, P.C. (2015) Epidemiology and diagnostic testing for hemochromatosis and iron overload. *Int. J. Lab. Hem.* **37**, 25–30 doi: 10.1111/ijlh.12347

13. Pietrangelo, A. (2010) Hereditary Hemochromatosis: Pathogenesis, diagnosis, and treatment. *Gastroenterology* **139,** 393–408 doi: 10.1053/j.gastro.2010.06.013

14. Feder, J.N., Gnirke, A., Thomas, W., Tsuchihashi, Z., Ruddy, D.A., Basava, A. et al. (1996) A novel MHC class I-like gene is mutated in patients with hereditary haemochromatosis. *Nat. Genet*. **13**, 399-408 doi: 10.1038/ng0896-399

15. Wu, X., Wang, Y., Wu, Q., Cheng, W., Liu, W., Zhao, Y. et al. (2014) HFE interacts with the BMP type I receptor ALK3 to regulate hepcidin expression. *Blood* **124**, 1355-1343 doi: 10.1182/blood-2014-01-552281

16. Bridle, K.R., Frazer, D.M., Wilkins, S.J., Dixon, J.L., Purdie, D.M., Crawford, D.H.G. et al. (2003) Disrupted hepcidin regulation in HFE-associated haemochromatosis and the liver as a regulator of body iron homoeostasis. *Lancet* **361**, 669–73 doi: 10.1016/S0140-6736(03)12602-5

17. Nemeth, E., Tuttle, M.S., Powelson, J., Vaughn, M.B., Donovan, A., Ward, D.M. et al. (2004) Hepcidin regulates cellular iron efflux by binding to ferroportin and inducing its internalization. *Science* **306**, 2090-2093 doi: 10.1126/science.1104742

18. Schumacher, H.R., Jr. Arthropathy in hemochromatosis. *Hosp. Pract*. **33,** 81-86 doi: 10. 1080/21548331.1998.11443654

19. McDonnell, S.M., Preston, B.L., Jewell, S.A., Barton, J.C., Edwards C.Q., Adams, P.C. et al. (1999) A survey of 2,851 patients with hemochromatosis: symptoms and response to treatment. *Am. J. Med*. **106,** 19-24.

20. Ross, J.M., Kowalchuk, R.M., Shaulinsky, J., Ross, L., Ryan, D., Phatak, P.D. (2003) Association of heterozygous hemochromatosis C282Y gene mutation with hand osteoarthritis. *J. Rheumatol*. **30,** 121-125.

21. Timms, A.E., Sathananthan, R., Bradbury, L., Athanassou, N.A., Wordsworth, B.P., Brown, M.A. (2002) Genetic testing for haemochromatosis in patients with chondrocalcinosis. *Ann. Rheum. Dis*. **61,** 745-747 doi: 10. 1136/ard.61.8.745

22. Willis, G., Scott, D.G., Jennings, B.A., Smith, K., Bukhari, M., Wimperis, J.Z. (2002) HFE mutations in an inflammatory arthritis population. *Rheumatology (Oxford)* **41,** 176-179 doi: 10. 1093/rheumatology/41.2.176

23. Rovetta, G., Grignolo, M.C., Buffrini, L., Monteforte, P. (2002) Prevalence of C282Y mutation in patients with rheumatoid arthritis and spondylarthritis. *Int. J. Tissue. React*. **24,** 105-109.

24. Lambert, R.E. (2001) Iron storage diseases. In: Kelley's Textbook of Rheumatology (eds. Ruddy, S., Harris, E.D., Sledge, C.B.), 6th edition, 1559-1565. Philadelphia: WB Saunders.

25. Brighton, C.T., Bigley, E.C., Jr., Smolenski, B.I. (1970) Iron-induced arthritis in immature rabbits. *Arthritis Rheum*. **13,** 849-857.

26. Bhutia, Y.D., Ogura, J., Grippo, P.J., Torres, C., Sato, T., Wachtel, M. et al. (2020) Chronic exposure to excess iron promotes EMT and cancer via p53 loss in pancreatic cancer. *Asian J. Pharm. Sci*. (in press).

27. Kim, J.S., Lee, C., Bonifant, C.L., Ressom, H., Waldman, T. (2007) Activation of p53-dependent growth suppression in human cells by mutations in PTEN or PIK3CA. *Mol. Cell. Biol*. **27**, 662-77 doi: 10.1128/MCB.00537-06

28. Loughery, J., Cox, M., Smith, L.M., Meek, D.W. (2014) Critical role for p53-serine 15 phosphorylation in stimulating transactivation at p53-responsive promoters. *Nucleic Acids Res.* **42**, 7666-80. doi: 10.1093/nar/gku501

29. Kang, D.H., Nakagawa, T., Feng, L., Watanabe, S., Han, L., Mazzali, M., *et al.* (2002) A role for uric acid in the progression of renal disease. *J. Am. Soc. Nephrol*. **13**, 2888-97. doi: 10.1097/01.asn.0000034910.58454.fd

30. Kratzer, J.T., Lanaspa, M.A., Murphy, M.N., Cicerchi, C., Graves, C.L., Tipton, P.A. et al. (2014) Evolutionary history and metabolic insights of ancient mammalian uricases. *Proc. Natl. Acad. Sci. (USA)* **111**, 3763-3768. doi: 10.1073/pnas.1320393111

31. Pritsos, C.A. (2000) Cellular distribution, metabolism and regulation of the xanthine oxidoreductase enzyme system. *Chem. Biol. Interact*. **1,** 195-208 doi: 10.1016/s0009-2797(00)00203-9

32. Okamoto, K., Kusano, T., Nishino, T. (2013) Chemical nature and reaction mechanisms of the molybdenum cofactor of xanthine oxidoreductase. *Curr. Pharmaceut. Design* **19**, 2606-2614 doi: 10.2174/1381612811319140010

33. Reginato, A.M., Mount, D.B., Yang, I., Choi, H.K. (2012) The genetics of hyperuricaemia and gout. *Nat. Rev. Rheumatol.* **8**, 610-21 doi: 10.1038/nrrheum.2012.144

34. Hosomi, A., Nakanishi, T., Fujita, T., Tamai, I. (2012) Extra-renal elimination of uric acid via intestinal efflux transporter BCRP/ABCG2. *PLoS One* **7**, e30456 doi: 10.1371/journal.pone.0030456

35. Woodward, O.M., Köttgen, A., Coresh, J., Boerwinkle, E., Guggino, W.B., Köttgen, M. (2009) Identification of a urate transporter, ABCG2, with a common functional polymorphism causing gout. *Proc. Natl. Acad. Sci. USA* **106**, 10338-10342 doi: 10.1073/pnas.0901249106

36. Nakanishi, T., Ross, D.D. (2012) Breast cancer resistance protein (BCRP/ABCG2): its role in multidrug resistance and regulation of its gene expression. *Chin. J. Cancer*. **31**, 73-99. doi: 10.5732/cjc.011.10320

37. Nakanishi, T., Bailey-Dell, K.J., Hassel, B.A., Shiozawa, K., Sullivan, D.M., Turner, J., *et al.* (2006) Novel 5' untranslated region variants of BCRP mRNA are differentially expressed in drug-selected cancer cells and in normal human tissues: implications for drug resistance, tissue-specific expression, and alternative promoter usage. *Cancer Res.* **66**, 5007-11. doi: 10.1158/0008-5472.CAN-05-4572

38. Zong, Y., Zhou, S., Fatima, S., Sorrentino, B.P. (2006) Expression of mouse Abcg2 mRNA during hematopoiesis is regulated by alternative use of multiple leader exons and promoters. *J. Biol. Chem*. **281**, 29625-32. doi:10.1074/jbc.M606314200

39. Shen, J., Sheng, X., Chang, Z., Wu, Q., Wang, S., Xuan, Z. et al. (2014) Iron metabolism regulates p53 signaling through direct heme-p53 interaction and modulation of p53 localization, stability, and function. *Cell Rep*. **7**, 180-93 doi: 10.1016/j.celrep.2014.02.042

40. Wang, X., Wu, X., Wang, C., Zhang, W., Ouyang, Y., Yu, Y. et al. (2010) Transcriptional suppression of breast cancer resistance protein (BCRP) by wild-type p53 through the NF-kappaB pathway in MCF-7 cells. *FEBS Lett.* **584**, 3392-7 doi: 10.1016/j.febslet.2010.06.033

41. Van Aubel, R.A., Smeets, P.H., van den Heuvel, J.J., Russel, F.G. (2005) Human organic anion transporter MRP4 (ABCC4) is an efflux pump for the purine end metabolite urate with multiple allosteric substrate binding sites. *Am. J. Physiol. Renal. Physiol.* **288**, F327-33. doi:10.1152/ajprenal.00133.2004.

42. Bataille, A.M., Goldmeyer, J., Renfro, J.L. (2008) Avian renal proximal tubule epithelium urate secretion is mediated by Mrp4. *Am. J. Physiol. Regul. Integr. Comp. Physiol.* **295**, R2024–R2033. doi:10.1152/ajpregu.90471.2008.

43. Bobulescu, I.A., Moe, O.W. (2012) Renal transport of uric acid: Evolving concepts and uncertainties. *Adv. Chronic Kidney Dis.* **19**, 358–371. doi:10.1053/j.ackd.2012.07.009.

44. Tanner, C., Boocock, J., Stahl, E.A, Dobbyn, A., Mandal, A.K., Cadzow, M. (2017) Population specific resequencing associates the ATP Binding Cassette Subfamily C Member 4 (ABCC4) gene with gout in New Zealand Māori and Pacific men. *Arthritis Rheumatol.* **69,** 1461-1469. doi:10.1002/art.40110.

45. Flais, J., Bardou-Jacquet, E., Deugnier, Y., Coiffier, G., Perdriger, A., Chalès, G. et al. (2017) Hyperferritinemia increases the risk of hyperuricemia in HFE-hereditary hemochromatosis. *Joint Bone Spine* **84**, 293-297 doi: 10.1016/j.jbspin.2016.05.020

46. Ghio, A.J., Ford, E.S., Kennedy, T.P., Hoidal, J.R. (2005) The association between serum ferritin and uric acid in humans. *Free Radic. Res.* **39**, 337-42 doi: 10.1080/10715760400026088

47. Chen, S.C.C., Huang, Y.F., Wang, J.D. (2012) Hyperferritinemia and hyperuricemia may be associated with liver function abnormality in obese adolescents. *PLoS One* **7**, e48645 doi: 10.1371/journal.pone.0048645

48. Ghio, A. J., Kennedy, T. P., Rao, G., Cooke, C. L., Miller, M. J., Hoidal, J. R. (1994) Complexation of iron cation by sodium urate crystals and gouty inflammation. *Arch. Biochem. Biophys.* 313: 215-221.

49. DeBosch, B.J., Kluth, O., Fujiwara, H., Schürmann, A., Moley, K. (2014) Early-onset metabolic syndrome in mice lacking the intestinal uric acid transporter SLC2A9. *Nat. Commun.* **7**, 4642 doi: 10.1038/ncomms5642

50. Wang, H., Zhang, H., Sun, L., Guo, W. (2018) Roles of hyperuricemia in metabolic syndrome and cardiac-kidney-vascular system diseases. *Am. J. Transl. Res*. **10**, 2749–2763 ISSN:1943-8141/AJTR0075539

51. Oh, T.R., Choi, H.S., Kim, C.S., Bae, E.H., Ma, S.K., Sung, S.A. et al. (2019) Hyperuricemia has increased the risk of progression of chronic kidney disease: propensity score matching analysis from the KNOW-CKD study. *Sci. Rep.* **30**, 6681 doi: 10.1038/s41598-019-43241-3

52. Li, Y., Xu, C., Yu, C., Xu, L., Miao, M. (2009) Association of serum uric acid level with non-alcoholic fatty liver disease: a cross-sectional study. *J. Hepatol.* **50**, 1029-34 doi: 10.1016/j.jhep.2008.11.021

Figure legends

Figure 1. Systemic and organ-specific accumulation of UA in *Hfe*$^{-/-}$ mice. UA concentration was measured in (**A**) serum, (**B**) ileum, and (**C**) colon in *Hfe*$^{-/-}$ mice and their wild type counterparts using UA Assay Kit. Mice used in the study were 14-months old. Data show mean values of three mice per group ± SEM. $^{**}P < 0.01$, $^{***}P < 0.001$.

Figure 2. Activity of XO, but not its expression, is significantly increased in *Hfe*$^{-/-}$ mouse liver and small intestine. (**A**) Quantitative PCR analysis of XO mRNA in liver and intestinal segments of wild type mouse. Data show mean values ± SEM relative to liver, which is taken as 1. $^{****}P < 0.0001$; ns, not significant. (**B**) Western blot for XO protein levels in liver and intestinal segments of wild type mouse. Western blot band intensities were estimated using ImageJ software and the band intensities were normalized to the respective β-tubulin band intensities. Please see Supplementary Figures S4 and S5 for full blot images. (**C**) Quantitative PCR analysis of XO mRNA in liver, jejunum, ileum, and colon of *Hfe*$^{-/-}$ mice and wild type mice. Data show mean values of three mice per group ± SEM relative to control mice. $^{*}P < 0.05$. (**D**) Western blot for XO protein levels in *Hfe*$^{-/-}$ and wild type liver and jejunum. Western blot band intensities were estimated using ImageJ software and the band intensities were normalized to the respective β-actin band intensities. Please see Supplementary Figure S6, S7, S8, and S9 for full blot images. (**E**) XO activity in wild type and *Hfe*$^{-/-}$ mice. Data show the mean of three mice per group ± SEM. $^{**}P < 0.01$; $^{***}P < 0.001$.

Figure 3. Expression of Glut9 and MRP4 in wild type and *Hfe*$^{-/-}$ mouse liver and intestinal tract. (**A**) Quantitative PCR analysis of Glut9 mRNA in liver and intestinal segments of wild type mouse. Data show mean values ± SEM relative to liver, which is taken as 1. $^{*}P < 0.05$; $^{***}P < 0.001$. (**B**) Western blot for Glut9 protein levels in liver and intestinal segments of the wild type mouse. Western blot band intensities were estimated using ImageJ software and the band intensities were normalized to the respective β-tubulin band intensities. Please see Supplementary Figures S5 and S10 for full blot images. (**C**) Quantitative PCR of Glut9 mRNA in liver, jejunum, ileum, and colon of *Hfe*$^{-/-}$ mice and wild type mice. Data show mean values of three mice per group ± SEM relative to control mice. (**D**) Western blot for Glut9 protein levels in *Hfe*$^{-/-}$ mouse and wild type mouse liver, jejunum, ileum, and colon. Western blot band intensities were estimated using ImageJ software and the band intensities were normalized to the respective β-actin band intensities. Please see Supplementary Figures S8, S9, and S11 for full blot images. (**E**) Quantitative PCR analysis of Mrp4 mRNA in liver and intestinal segments of wild type mouse. Data show mean values ± SEM relative to liver, which is taken as 1. $^{*}P < 0.05$; $^{***}P < 0.001$. (**F**) Quantitative PCR analysis of Mrp4 mRNA in liver, jejunum, ileum, and colon of *Hfe*$^{-/-}$ mice and wild type mice. Data show mean values of three mice per group ± SEM relative to control mice. $^{**}P < 0.01$.

Figure 4. Abcg2 is robustly expressed in mouse intestine. (**A**) Quantitative PCR analysis of Abcg2 mRNA in kidney, liver, and intestinal segments of wild type mouse. Data show mean values ± SEM relative to kidney, which is taken as 1. $^{****}P < 0.0001$. (**B**) Western blot for Abcg2 protein levels in intestinal segments of wild type mouse. Western blot band intensities were estimated using ImageJ software and the band intensities were normalized to the respective β-actin band intensities. Please see Supplementary Figure S12 for a full blot image. (**C**) UA was measured in serum of *Abcg2*$^{-/-}$ mice and wild type mice. Mice used in the study were 7-months old. Data show mean values of three mice per group ± SEM. $^{*}P < 0.05$.

Figure 5. Abcg2 is downregulated in *Hfe*$^{-/-}$ mouse intestine. (**A**) Quantitative PCR analysis of Abcg2 mRNA in colon epithelium of *Hfe*$^{-/-}$ mice and wild type mice. Data show mean values of three mice per group ± SEM relative to control mice. $^{**}P < 0.01$. (**B**) Western blot for Abcg2 protein levels in ileal and colonic epithelium from wild type and *Hfe*$^{-/-}$ mice. Please see Supplementary Figures S13 and S14 for full blot images. Western blot band intensities were estimated using ImageJ software and the band intensities that correspond to the Abcg2 protein were normalized to the respective β-actin levels in (**C**) ileal epithelium and (**D**) colonic epithelium. Data represent mean values of three mice per group ± SEM. $^{**}P < 0.01$.

Figure 6. ChIP analysis of p53 binding to human *ABCG2* gene promoter. (**A**) p53 consensus sequences in h*ABCG2* and m*Abcg2* gene promoters as assessed with JASPAR software. A putative transcription start site (+1) was recognized at the start of the exon 1. Chromosomal locations for this transcription start site and also for p53 consensus sequences are shown. E1A or E1a, E1B or E1b, and E1C or E1c depict the transcript splice variants found in human ABCG2 gene or mouse Abcg2 gene, which result from the alternative promoter usage. (**B**) ChIP analysis for binding of p53 to the h*ABCG2* promoter. Experiment was performed in normal human epithelial cell line CCD841 transfected with either empty vector (pLKO.1) or a vector containing shRNA that targets p53 mRNA. shRNA efficiency was estimated by observing p53 protein levels via western blot. Please see Supplementary Figures S15, S16, S17, S18, S19, S20, and S21 for full blot and agarose gel images. Data show the mean values of three independent experiments ± SEM. $^{*}P < 0.05$; $^{**}P < 0.01$.

Figure 7. p53 protein levels are significantly decreased in *Hfe*$^{-/-}$ mouse ileum and colonic epithelium. Western blot for p53 protein in (**A**) ileal and (**C**) colonic epithelium of wild type and *Hfe*$^{-/-}$ mice. Please see Supplementary Figures S13 and S14 for full blot images. Western blot band intensities were estimated using ImageJ software and the band intensities that correspond to p53 protein were normalized to β-actin levels in (**B**) ileal epithelium and (**D**) colonic epithelium. Data represent mean values of three mice per group ± SEM. $^{**}P < 0.01$.

Figure 8. Schematic illustration of the differences in intestinal handling of uric acid between wild type and *Hfe*$^{-/-}$ enterocytes.

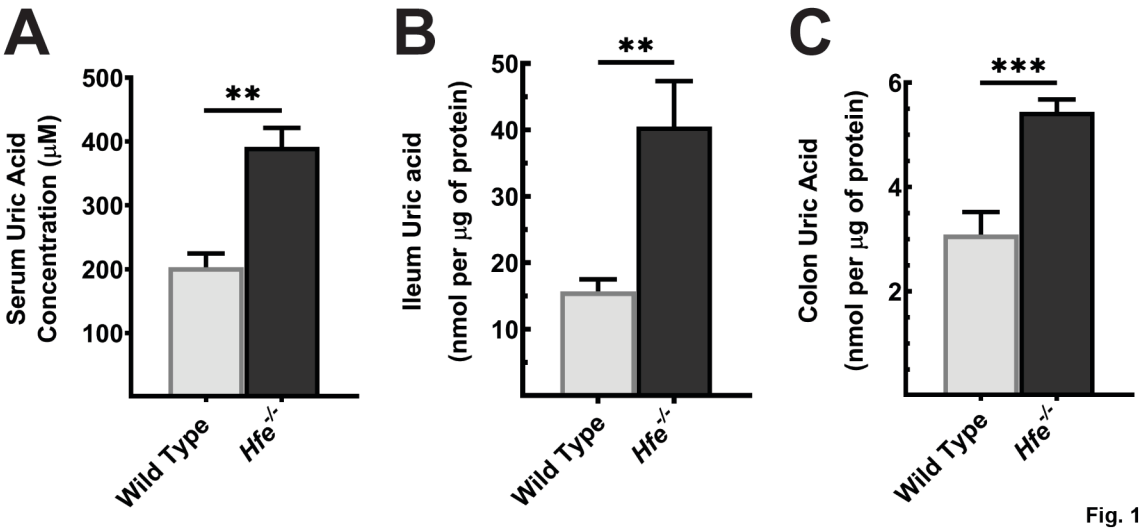

Fig. 1

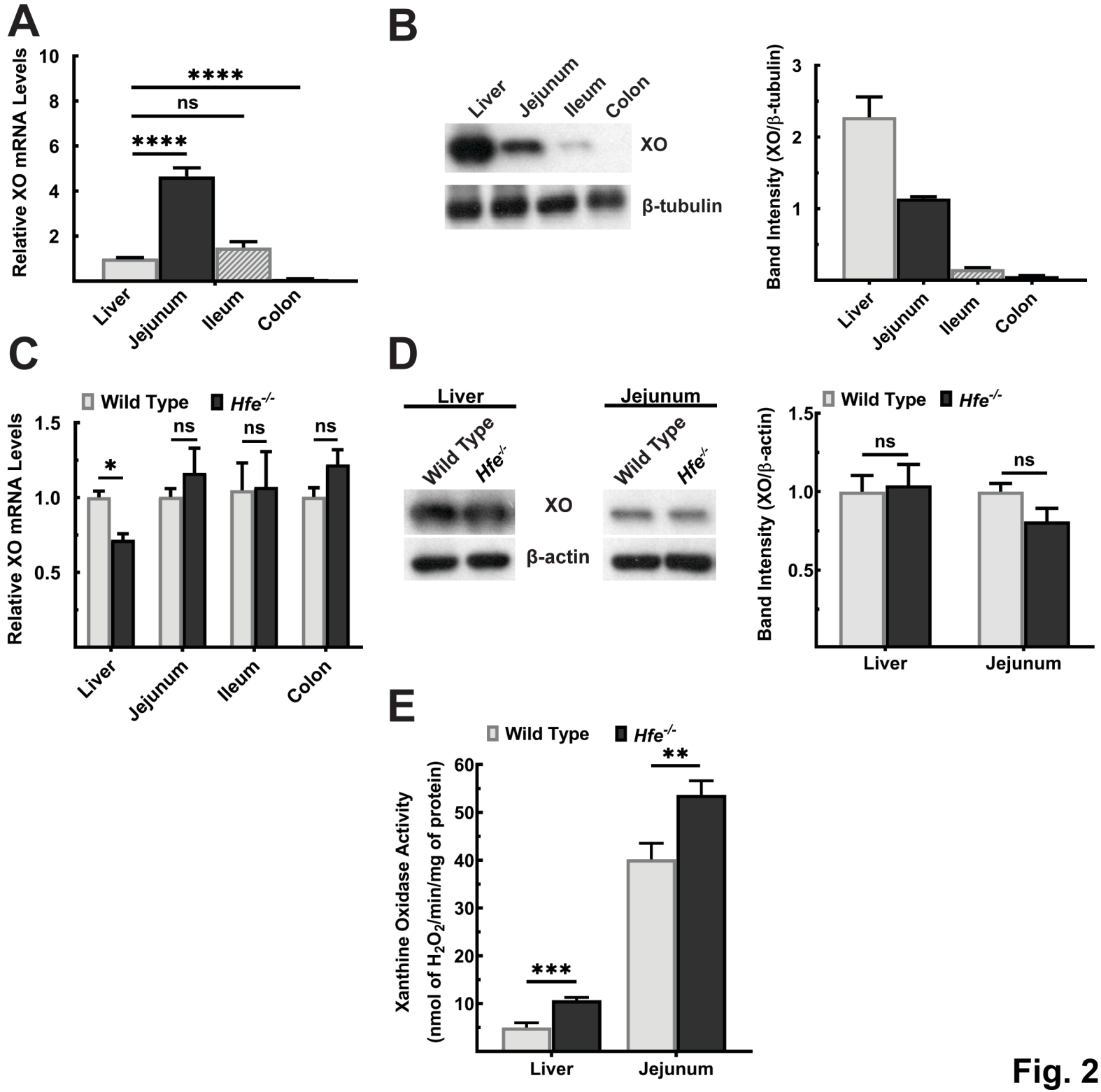

Fig. 2

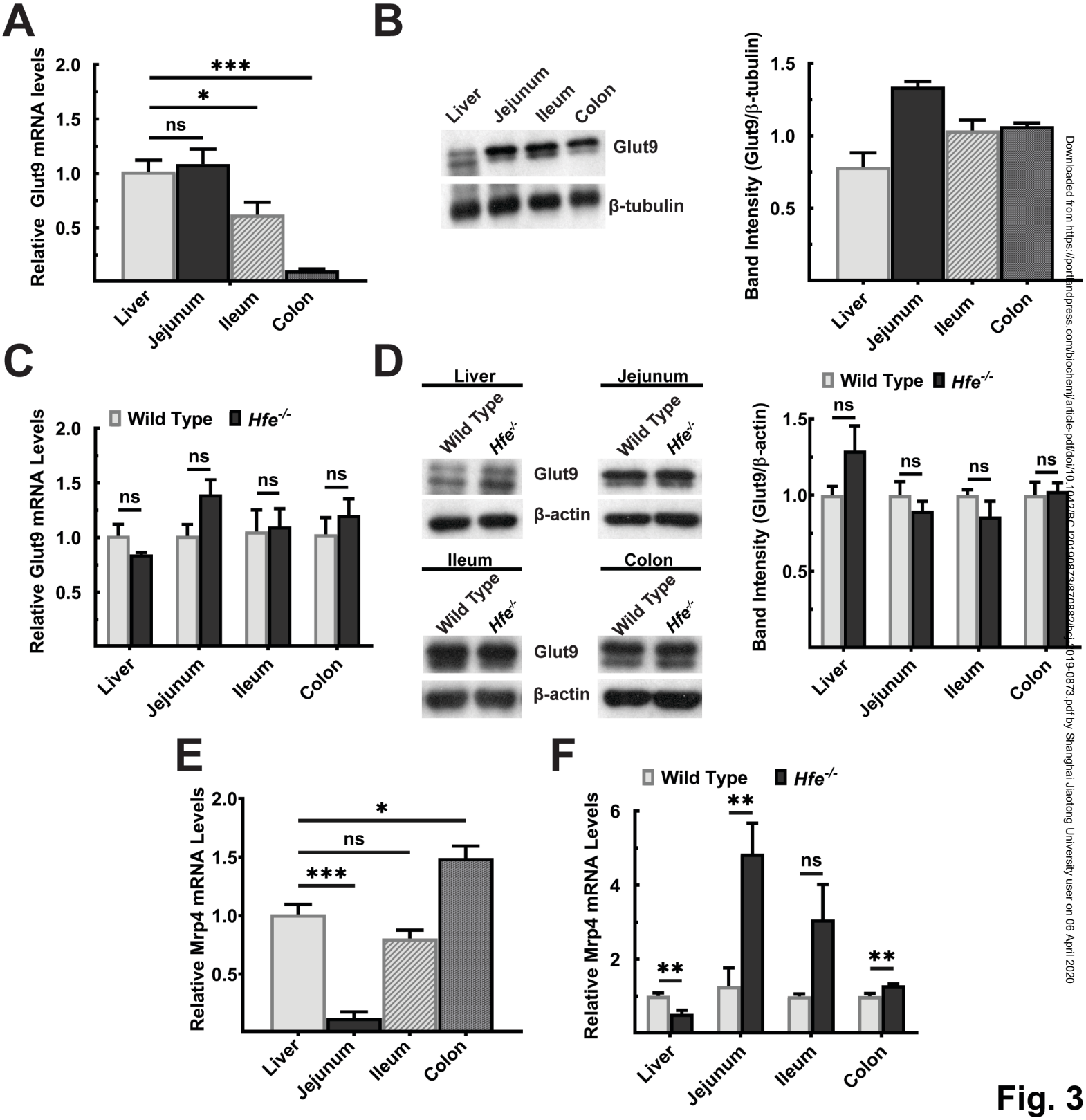

Fig. 3

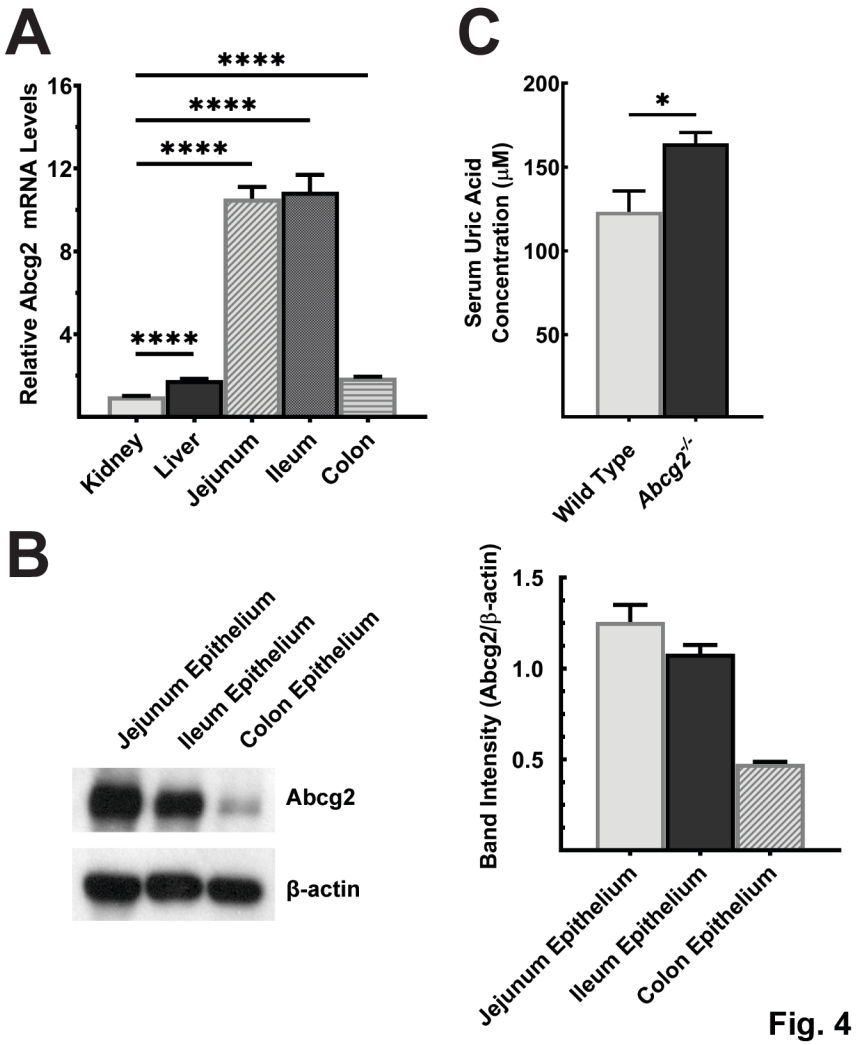

Fig. 4

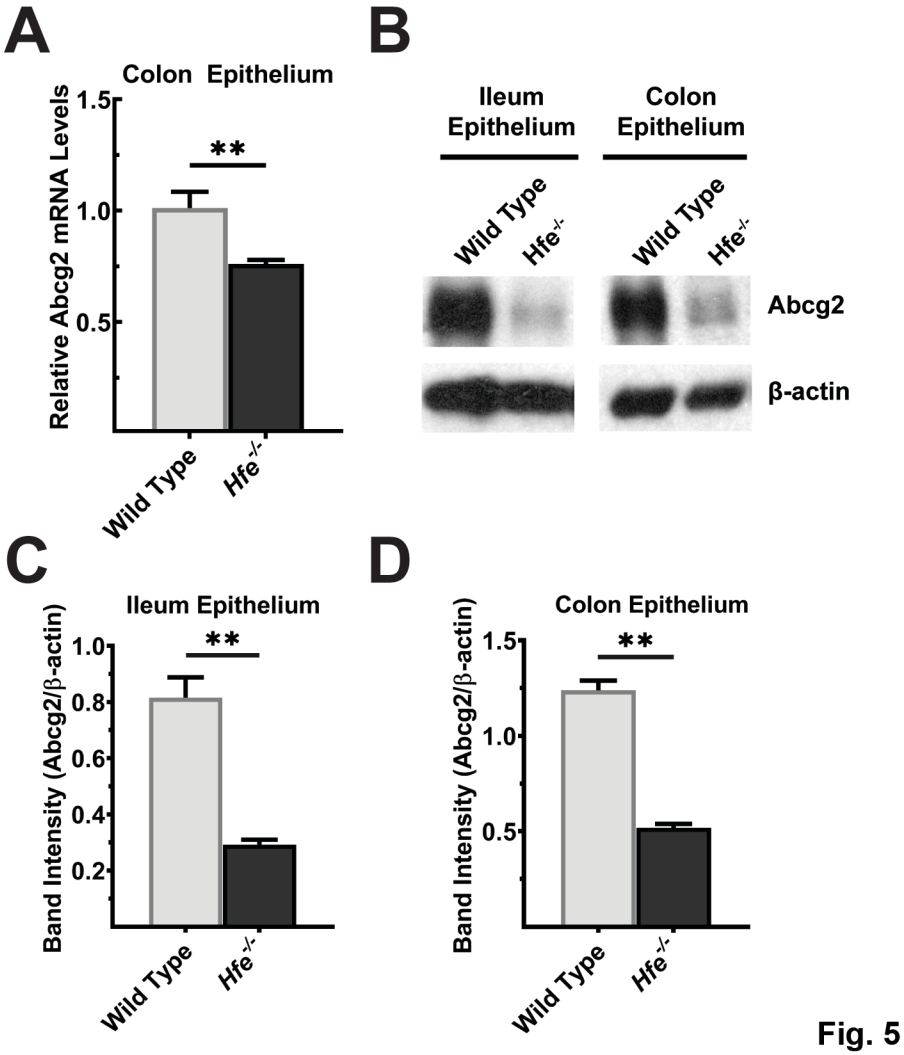

Fig. 5

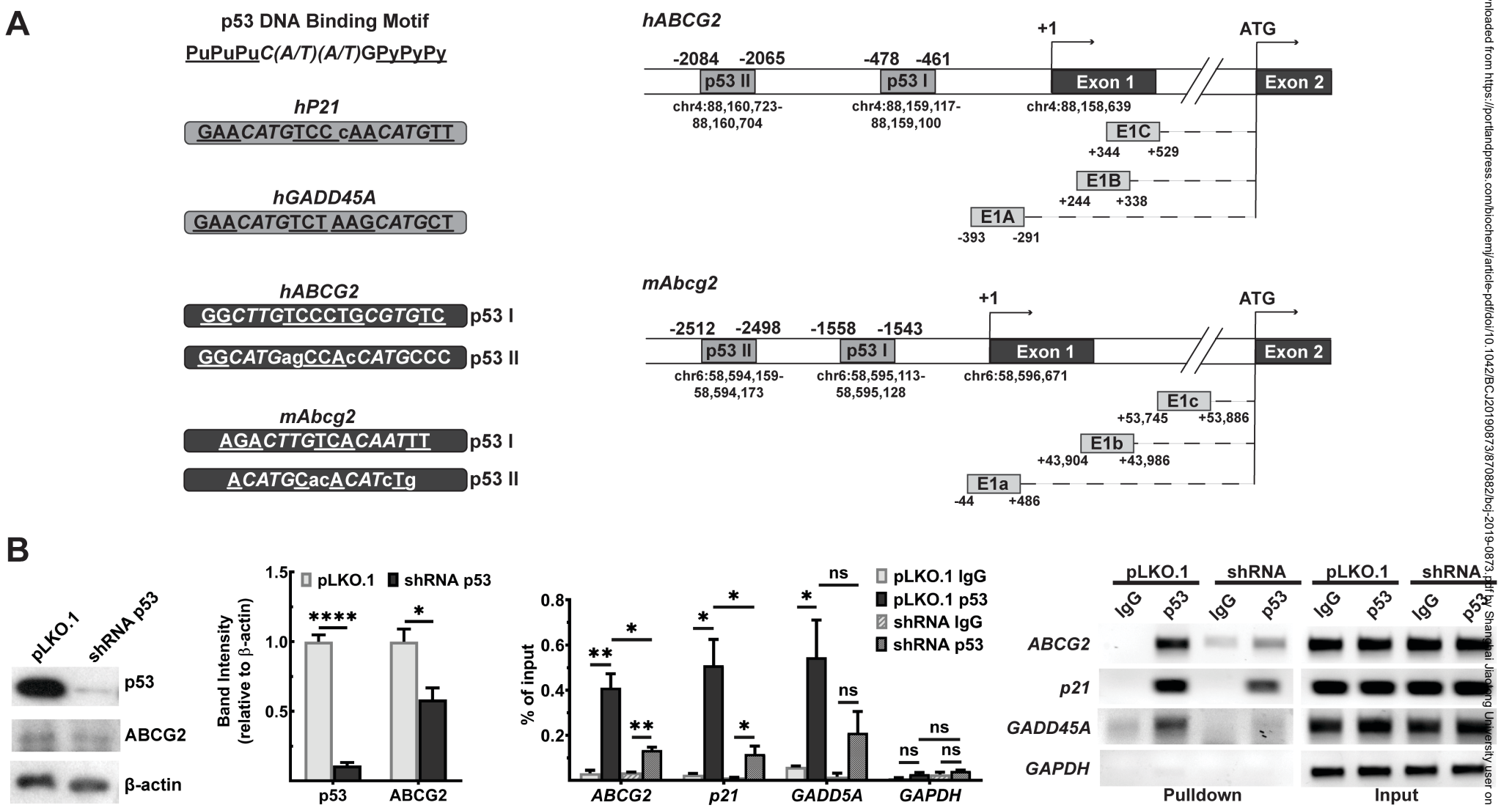

Fig. 6

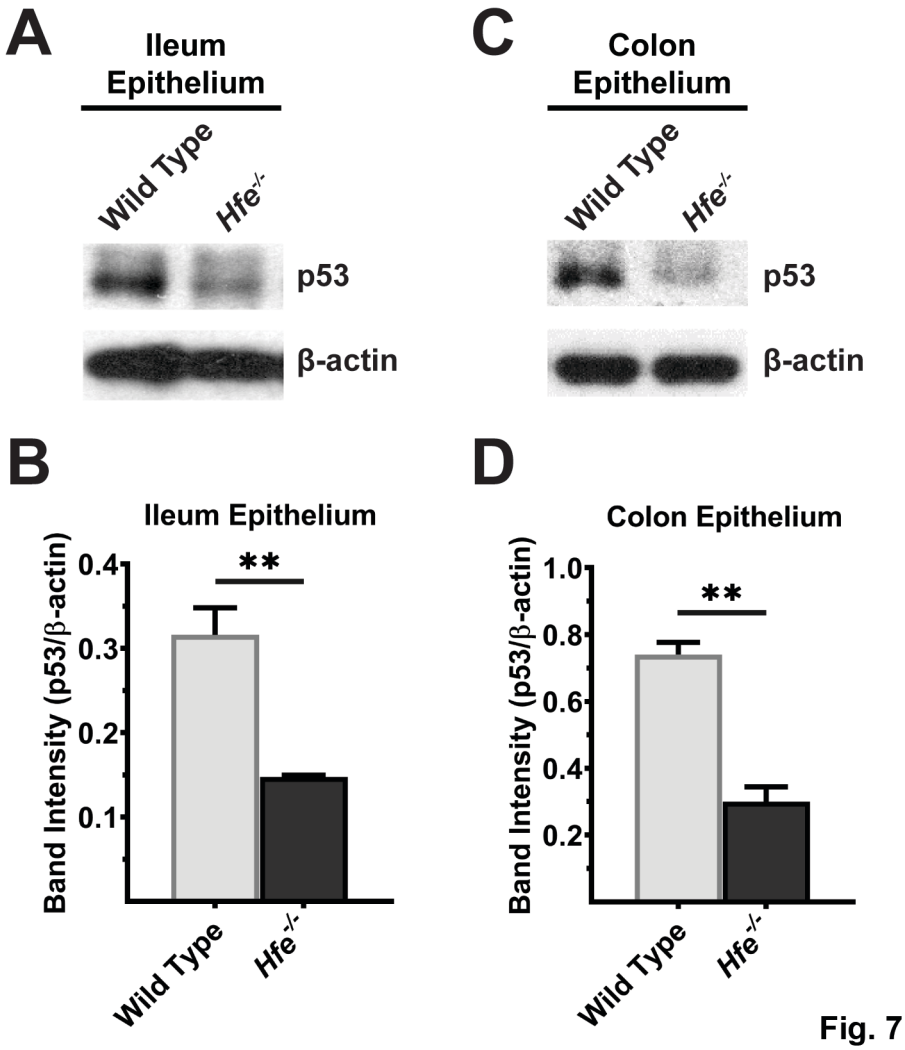

Fig. 7

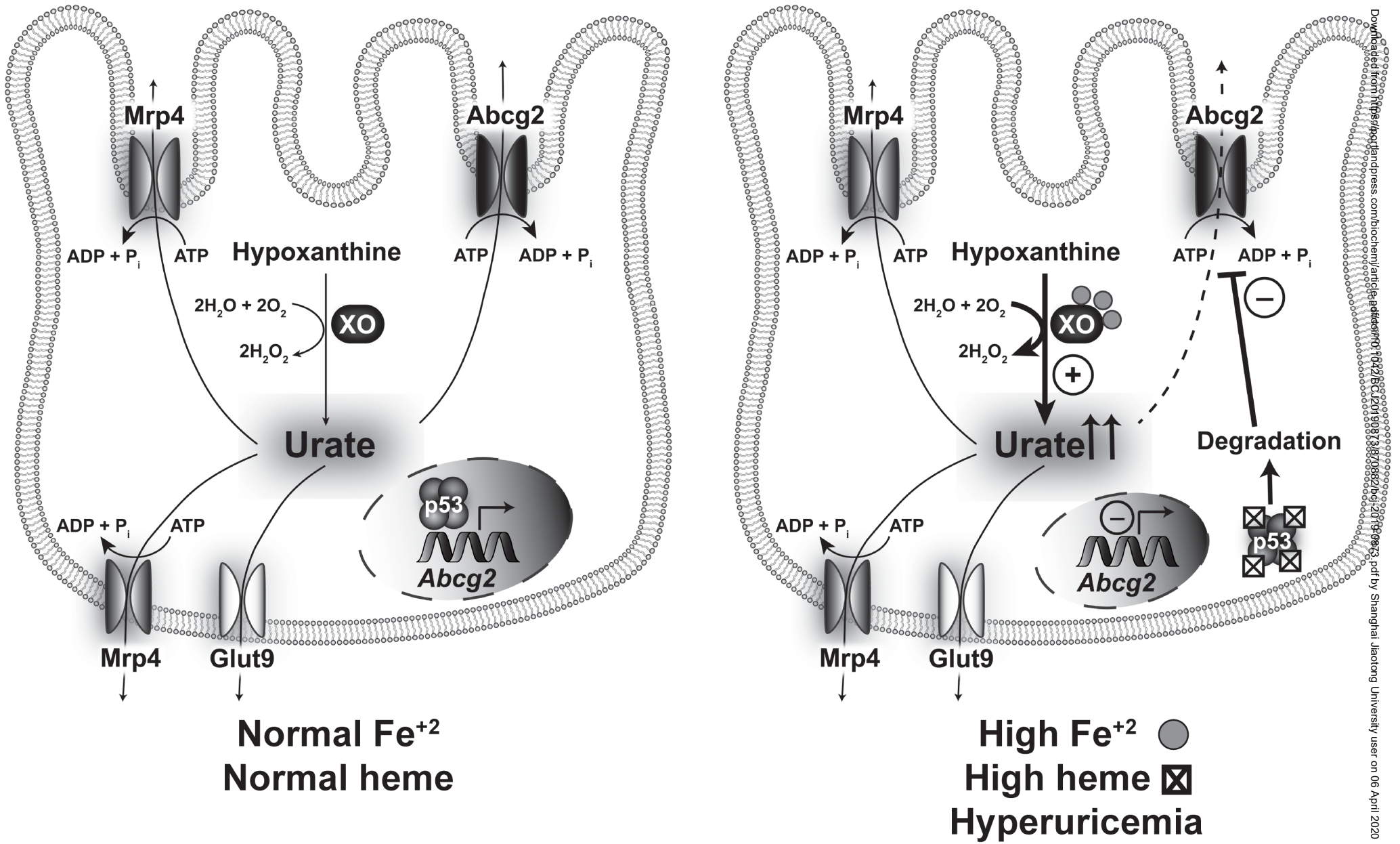

Fig. 8